JACS
JOURNAL OF THE AMERICAN CHEMICAL SOCIETY
Article
pubs.acs.org/JACS

Impact of Preferential Indium Nucleation on Electrical Conductivity of Vapor–Liquid–Solid Grown Indium–Tin Oxide Nanowires

Gang Meng,[†] Takeshi Yanagida,*[,†] Kazuki Nagashima,[†] Hideto Yoshida,[†] Masaki Kanai,[†] Annop Klamchuen,[†] Fuwei Zhuge,[†] Yong He,[†] Sakon Rahong,[†] Xiaodong Fang,[‡] Seiji Takeda,[†] and Tomoji Kawai*[,†]

[†]Institute of Scientific and Industrial Research, Osaka University, 8-1 Mihogaoka, Ibaraki, Osaka 567-0047, Japan
[‡]Anhui Institute of Optics and Fine Mechanics, Chinese Academy of Sciences, Hefei 230031, China

Supporting Information

ABSTRACT: Highly conductive and transparent indium–tin oxide (ITO) single-crystalline nanowires, formed by the vapor–liquid–solid (VLS) method, hold great promise for various nanoscale device applications. However, increasing an electrical conductivity of VLS grown ITO nanowires is still a challenging issue due to the intrinsic difficulty in controlling complex material transports of the VLS process. Here, we demonstrate a crucial role of preferential indium nucleation on the electrical conductivity of VLS grown ITO nanowires using gold catalysts. In spite of the fact that the vapor pressure of tin is lower than that of indium, we found that the indium concentration within the nanowires was always higher than the nominal composition. The VLS growth of ITO through gold catalysts significantly differs from ITO film formations due to the emergence of preferential indium nucleation only at a liquid–solid interface. Furthermore, we demonstrate that the averaged resistivity of ITO nanowires can be decreased down to 2.1×10^{-4} Ω cm, which is the lowest compared with values previously reported, via intentionally increasing the tin concentration within the nanowires.

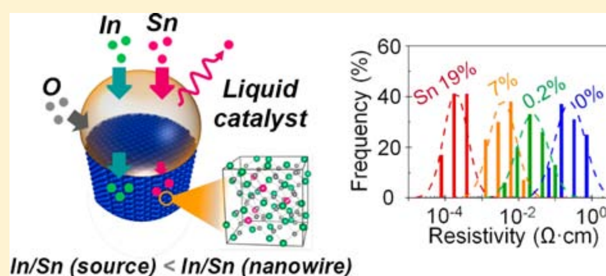

INTRODUCTION

A vapor–liquid–solid (VLS) method is one of the most powerful techniques to synthesize well-defined single-crystalline nanowires for various inorganic materials.[1−3] Among various inorganic nanowires, metal oxide nanowires exhibit fascinating physical properties, which are hardly attainable to other conventional semiconductor nanowires.[4−6] For example, indium–tin oxide (ITO) single-crystalline nanowires offer an excellent metallic conductivity with the transparency. Since a high conductance of single crystalline ITO nanowires is desirable for most applications of ITO, increasing further the conductivity of ITO nanowires will open up novel device applications,[7,8] where other conductive nanowires such as silver have been utilized.[9] Unfortunately, controlling the transport properties of VLS grown ITO nanowires is still a challenging issue due to the intrinsic difficulty in understanding the material transport phenomena during VLS growth across three phases.[10−13] Previous works as to VLS grown oxide nanowires have highlighted the importance of the vapor pressure of metal elements to control the nanowire composition during VLS nanowire formation.[14,15] For example, Sb-doped SnO_2 nanowires showed significant Sb desorption due to the relative high vapor pressure of Sb,[14] whereas Ta-doped SnO_2 nanowires exhibited Ta-rich shell layers due to the relative low vapor pressure of Ta.[15] According to this scenario, two metal elements, whose vapor pressures are similar, are ideal to fabricate multicomponent VLS oxide nanowires. ITO is such an ideal material, since the vapor pressures of indium and tin are relatively similar compared with above dopants such as Sb and Ta, as shown in the Supporting Information, Figure S1.[16] However, the incorporation dynamics of tin into In_2O_3 nanowires during the VLS process is still not well understood. These backgrounds motivated us to examine a VLS growth of ITO nanowires using gold catalysts and the effect on the electrical conductivity. We found that the nanowire growth of ITO through gold catalysts significantly differs from ITO film formations due to the emergence of preferential indium nucleation only at a liquid–solid interface. In addition, we show that the electrical conductivity of ITO nanowires can be enhanced by intentionally increasing the tin concentration within the nanowires.

EXPERIMENTAL SECTION

Tin-doped indium oxide (ITO) nanowires and indium-doped tin oxide nanowires were grown on MgO(100) and Al_2O_3(110) single-crystal substrates by the gold catalyst-assisted pulsed laser deposition technique (ArF excimer laser, λ = 193 nm),[17−25] respectively. SnO_2 and In_2O_3 mixed powders with tin atomic ratios Sn/(In + Sn) (hereafter noted as Sn atom %) of 1, 5, 10, 30, 50, and 90 atom % were milled and compressed to fabricate targets. The reason why we have

Received: February 22, 2013
Published: April 12, 2013

 © 2013 American Chemical Society

chosen a different oxide substrate for each nanowire is to evaluate the crystal structures of obtained nanowires by X-ray diffraction (XRD). Once the background pressure of the chamber was evacuated to be 5.0 $\times 10^{-6}$ Pa, oxygen and argon mixed gas was introduced into the chamber with the ambient total pressure of 10 Pa. The flux ratio of oxygen and argon was 1:1000.[14,15] Prior to the laser ablation, the gold (0.7 nm)-coated oxide substrate was preheated at the growth temperature of 750 °C for 20 min. After 60 min for nanowire growth, the samples were cooled down to room temperature (RT) within 30 min. The microstructure of the nanowires was characterized by field emission scanning electron microscopy (FESEM, JEOL JEM-7001F) at an accelerating voltage of 30 kV. High-resolution transmission electron microscopy (HRTEM, JEOL JEM-ARM200F) with X-ray energy dispersive spectroscopy (EDS) was used to evaluate the diameter, crystallinity, and macroscopic composition of the nanowires. HRTEM observation was performed at an accelerating voltage of 200 kV. Scanning transmission electron microscopy (STEM, JEOL JEM-ARM200F) at an acceleration voltage of 200 kV was employed to characterize the microscopic composition of the nanowires. The probe size was approximately 0.13 nm in JEM-ARM200F. To evaluate the transport properties of a single ITO nanowire, we utilized the following procedure. First, the ITO nanowires onto the substrate were sonicated and dispersed into isopropanol. Then, the nanowire suspension was dropped onto a phosphorus doped n-type silicon substrate capped with a thermally oxidized SiO_2 layer with 300 nm thickness. Electron beam lithography was used to define nanoscale electrode patterns on the SiO_2/Si substrate, followed by metal deposition of Pt/Au (20 nm/100 nm). The transport measurements were performed by using a semiconductor parameter analyzer (Keithley 4200SCS) over 20 nanowires for statistical reliability by varying the measurement temperatures from RT down to 77 K. ITO thin films were deposited on a MgO(100) substrate (without gold catalyst) at room temperature by a laser ablation of a SnO_2 and In_2O_3 mixed target. The metal flux, oxygen partial pressure, and total chamber pressure were the same as those for nanowire growth. After deposition, the composition of the thin film was measured by an electron probe microanalyzer (EPMA, JEOL, JXA-8800R).

■ RESULTS AND DISCUSSION

Figure 1a–d shows the SEM, XRD, and TEM-EDS data of fabricated ITO nanowires. These ITO nanowires were fabricated by using the target of Sn 10 atom %. As seen in XRD and TEM data, the nanowires only show the bixbyite structure of In_2O_3 not the rutile structure of SnO_2. The growth direction can be assigned to be [100]. STEM mapping images of ITO nanowires with the incorporated tin concentration of 20 atom % were shown in Figure 1e. The spatial distribution of tin within the nanowires is homogeneous, which is in fact a sharp contrast to the trend for Ta-doped SnO_2 nanowires, where a Ta-rich shell layer was preferentially formed on the nanowire sidewall via VS growth mode for the Ta species.[15] Thus, the relatively similar vapor pressures of tin and indium seem to allow us to create homogeneous multicomponent VLS nanowires, which is important for nanowire-based device applications.[26,27]

Within the framework of this scenario based on the vapor pressure of the metal element, indium-doped SnO_2 might be also a good candidate as homogeneous multicomponent VLS oxide nanowires. In addition, a first-principle calculation has predicted the emergence of p-type SnO_2 by doping indium as an acceptor.[28,29]

Figure 2a–e shows SEM, XRD, TEM-EDS, and STEM data of indium-doped SnO_2 (indium 10 atom %). Indium-doped SnO_2 nanowires were fabricated under a temperature of 750 °C and an oxygen partial pressure of 10^{-2} Pa. The indium-doped SnO_2 system exhibits the nanowire morphology with rutile structures of the SnO_2 compound. However, the composition analysis by TEM-EDS reveals that the indium concentration within the nanowires is extremely low and almost negligible even for samples using the target of the atomic ratio In/Sn = 10:90. Thus, the incorporation dynamics of dopants for indium-doped SnO_2 and tin-doped In_2O_3 are highly contrary. This discrepancy might be interpreted in terms of the solubility

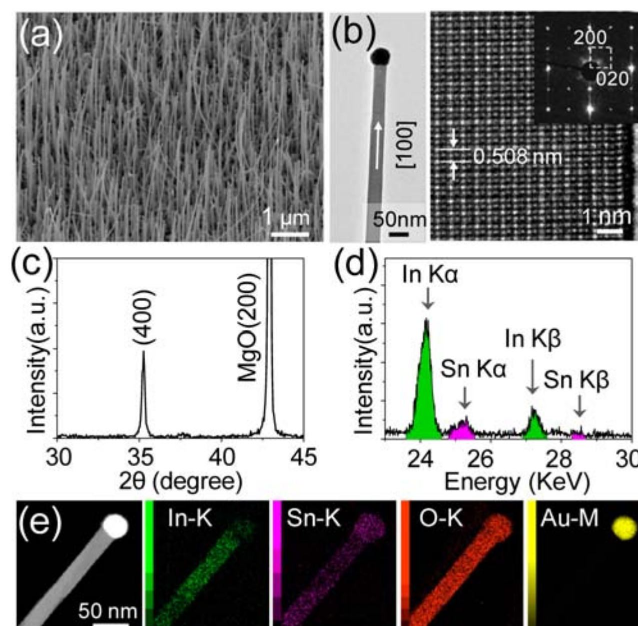

Figure 1. Morphology and microstructures of ITO nanowires (Sn 10 atom %). (a) FESEM image of nanowires grown on MgO(100) substrate; (b) TEM, HRTEM, and electron diffraction data; (c) XRD data of ITO nanowires; (d) TEM-EDS data of nanowires; (e) STEM elemental mapping images.

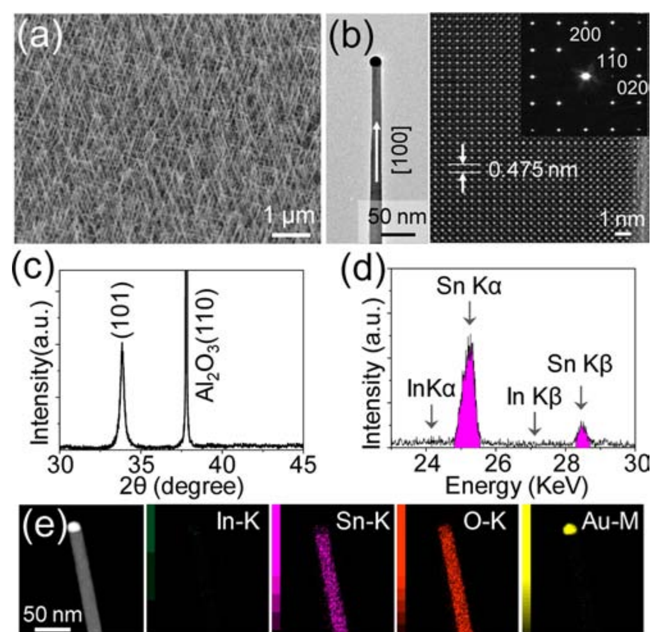

Figure 2. Morphology and microstructures of In-doped SnO_2 nanowires (Sn 90 atom %). (a) FESEM image of nanowires grown on Al_2O_3(110) substrate; (b) TEM, HRTEM, and electron diffraction data; (c) XRD data of nanowires; (d) TEM-EDS data of nanowires; (e) STEM elemental mapping images.

into parent compounds, since the bulk solubility of tin into In_2O_3 is significantly higher than that of indium into SnO_2.[30] The difference between In^{3+} and Sn^{4+} on the ionic radii (In^{3+} = 0.080 nm and Sn^{4+} = 0.069 nm for 6-fold coordination) might be the possible explanation for the different solubility.[31] Thus, the scenario based on only the vapor pressure of metal elements is not sufficient to realize a VLS growth of multicomponent oxide nanowires, but considering a solubility between different materials[32] is also required.

Figure 3 shows the tin concentration data within ITO nanowires, measured by TEM-EDS, when varying the nominal tin concentration of the target. Data ranging from 0 to 50 atom % are shown in the figure. Note that it is crucial to identify the presence and the concentration of tin within the nanowires via utilizing Sn K shell peaks rather than Sn L shell peaks due to the significant overlapping of tin and indium peaks. It can be clearly seen that the tin concentration within the nanowires is always lower than the nominal tin concentration. In the case of 10 atom % nominal composition, the tin concentration incorporated into the nanowires was about 5 atom %. Even for the highest tin nominal concentration 50 atom %, the tin concentration within the nanowires was about 18−20 atom %. These lower tin concentrations within the nanowires cannot be readily understood in terms of a conventional model based on the vapor pressure trends of metal elements during depositions[14,15] because the vapor pressure of tin is lower than that of indium for the temperature range employed here, for example, at 750 °C, 2.4×10^{-2} Pa for indium and 1.9×10^{-5} Pa for tin.[16] In other words, the indium concentration should be lower than that of tin if a re-evaporation causes the discrepancy of composition during depositions due to the vapor pressure difference. Our experimental trend in Figure 3 is also completely opposite to that of Sb-doped SnO_2 nanowires, where the higher vapor pressure of Sb resulted in the lower Sb concentration within nanowires due to the evaporation of Sb during VLS growth.[14]

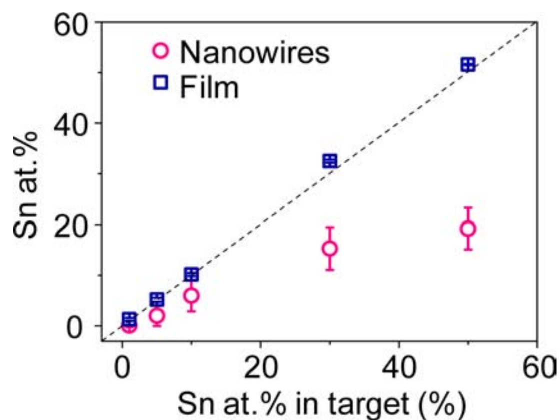

Figure 3. Composition data of ITO nanowires when varying tin concentrations in the target. Composition data measured from TEM-EDS are shown as a function of the nominal composition. For comparison, the composition data of ITO thin films grown under RT are also shown.

Here, we discuss what possibly causes the difference between the incorporated tin concentration within the nanowires and the nominal composition. First, we examine the composition ratio of indium and tin in the supplied flux. In order to measure such composition, we performed the EPMA composition measurements for ITO films deposited at RT, where the re-evaporation events are almost negligible.[14,15] Figure 3 shows the tin composition data of such RT grown ITO films as a function of nominal composition. As can be seen, the composition data of films are consistent with the nominal composition. Thus, the scenario based on the difference of the two metal compositions between the supplied flux and the target is not appropriate to explain our results. Second, we assume the difference between indium and tin on the incorporation probability into gold catalysts on the substrate surface. However, this scenario seems to be not consistent with the following experimental results. When we performed HRTEM analysis for nanowires using the target with the nominal compositions of Sn 50 atom %, we found precipitation of SnO_2 (rich) layers onto gold catalysts and also tin-rich cubic fluorite phases ($InSnO_{3.5}$, so-called ISO phase) just underneath the gold catalysts, as shown in Figure 4. A similar trend has been also reported in a previous report.[33,34] This result suggests that tin species are at least incorporated into gold catalysts during growth and the precipitation of tin from gold catalysts occurs during the cooling down process. In addition, the well-known VLS growth of SnO_2 nanowires using gold catalysts does not support the low incorporation probability of tin into gold catalysts.[35] Thus, the second scenario based on the incorporation probability into gold alone cannot give a rigorous explanation for our experimental observations.

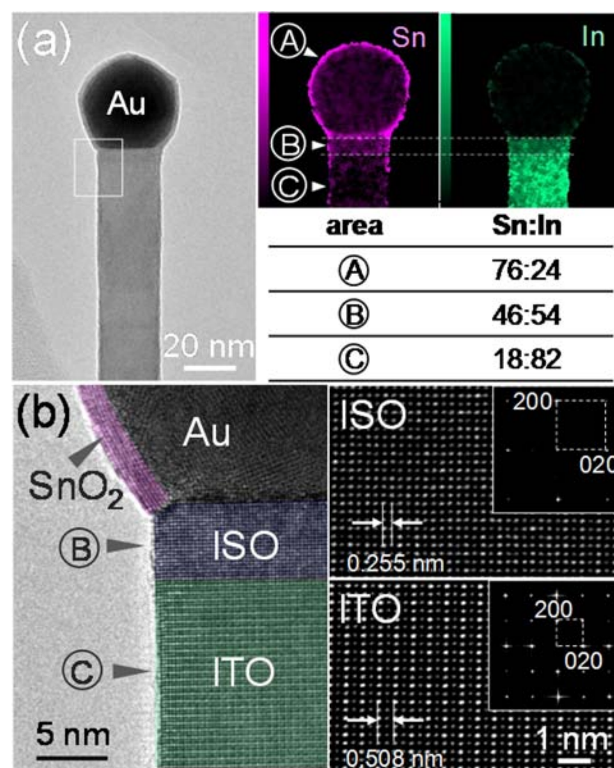

area	Sn:In
Ⓐ	76:24
Ⓑ	46:54
Ⓒ	18:82

Figure 4. HRTEM images of ITO nanowires (Sn 50 atom % in target). (a) TEM image of ITO nanowire and tin and indium STEM mapping around the gold catalyst; (b) HRTEM image of ITO nanowire near the gold catalyst, showing the presence of SnO_2 and ISO phases.

Finally, we consider a scenario based on the difference between indium and tin on the nucleation probability at a liquid−solid (LS) interface. This scenario assumes that indium

species within gold catalysts nucleate at the LS interface more preferentially than tin species. To examine this scenario, we compare the VLS growth rates of In_2O_3 and SnO_2 under the same experimental conditions. Table 1 shows the comparison

Table 1. Growth Rate of In_2O_3 and SnO_2 Nanowires[a]

	growth rate (nm/min)
In_2O_3	26.2
SnO_2	5.6

[a]Metal flux = 10^{17} cm^{-2} s^{-1}; oxygen partial pressure P_{O2} = 10^{-2} Pa; growth temperature T_{sub} = 750 °C.

between In_2O_3 and SnO_2 on the VLS growth rate. These nanowires were grown under a growth temperature of 750 °C, an oxygen partial pressure of 10^{-2} Pa, and a supplied metal flux of 10^{17} cm^{-2} s^{-1}. We have estimated the supplied metal flux by measuring the volume of thin films grown under RT. Clearly, the VLS growth rate of In_2O_3 was higher than that of SnO_2 under the same material flux. This experimental trend is consistent with the above scenario based on the higher nucleation rate of In_2O_3. This VLS growth rate dependence on materials might be understood in terms of a bonding energy of compounds, because there is a correlation between the bonding energy of compounds and the energy barrier for the nucleation process.[36] A melting point correlates with the bonding energy, that is, the higher the melting point, the lower the energy barrier for nucleation. The melting point for In_2O_3 is 1910 °C, and that for SnO_2 is 1630 °C. Thus, a nucleation rate of In_2O_3 at the LS interface can be faster than that of SnO_2 due to their possible different energy barriers for nucleation, that is, the lower activation energy for In_2O_3 nucleation.[36] This also explains why we have observed only ITO nanowires rather than SnO_2 nanowires even for 50 atom % target. Since a vapor−solid growth (i.e., sidewall growth) has not been observed for the experimental conditions employed,[35] tin species seem to re-evaporate than indium due to the lower nucleation rate at the LS interface. One of the possible explanations why there is a difference between the LS and VS interfaces on the nucleation barriers is based on the presence of liquid metal atoms at the LS interface and the interaction between the liquid metal atoms and the supplied metal atoms. This difference might cause the discrepancy between the LS and VS interfaces on the nucleation events. Thus, our results highlight that tailoring multicomponent VLS oxide nanowires strongly requires a consideration as to a nucleation probability at the LS interface, which has not been an issue for VLS growths of simple binary oxides.

Finally, we examine the effect of tin concentration on the transport properties of ITO nanowires. Figure 5a shows the *I*−*V* data of single ITO nanowire junctions (Pt/ITO/Pt) when varying the tin concentration. Figure 5b shows the distribution data of measured resistivity values to ensure the statistical difference between different tin concentrations. Figure 5c shows the correlation between the tin concentration incorporated into the nanowires and the resistivity. Clearly, there is a straightforward relationship between the incorporated tin concentration and the resistivity. The higher the tin concentration, the lower the resistivity due to increased carrier concentration. Thus, understanding the preferential nucleation of indium during ITO nanowire formation is essential to enhance the conductivity of ITO nanowires via increasing tin concentration of ITO nanowires. The averaged resistivity of

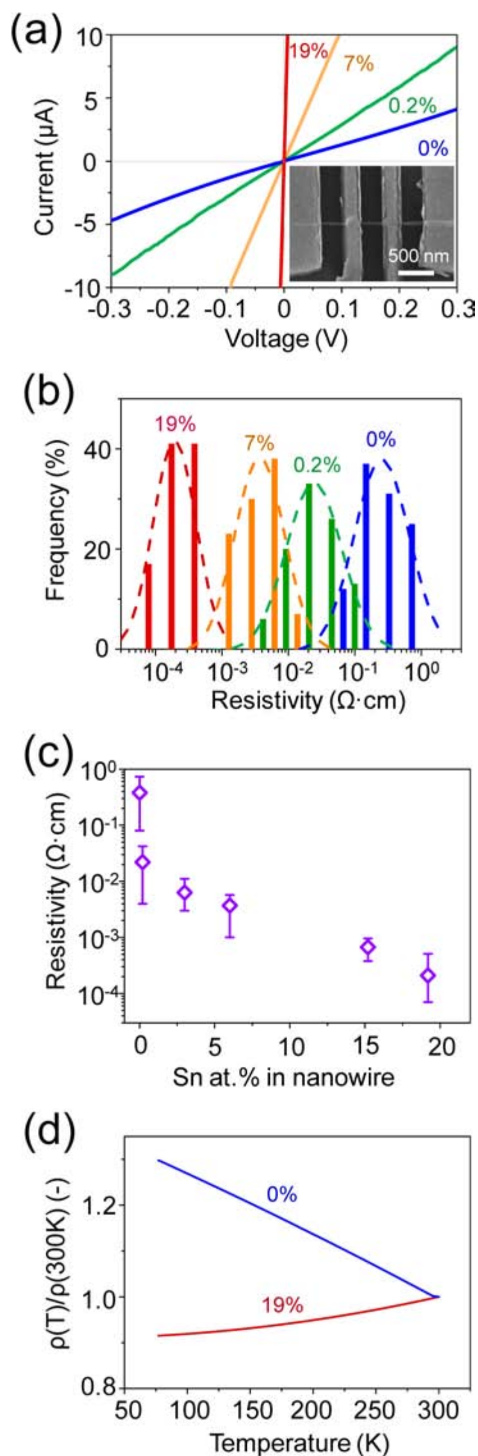

Figure 5. Transport properties of ITO nanowires with varying tin concentrations. (a) *I*−*V* data measured by a four-probe method at RT, and the inset shows the SEM image of the fabricated device; (b) resistivity distribution data; (c) relationship between tin concentration incorporated into ITO nanowires and the resistivity of ITO nanowires; (d) temperature dependence data.

ITO nanowires can be decreased down to 2.1 × 10^{-4} Ω cm, which is lower than the resistivity values of ITO nanowires previously reported.[37−40] Although the typical averaged resistivity of VLS grown ITO nanowires has been reported to be around 10^{-3} Ω cm up to 10^{-1} Ω cm,[33,35] the discrepancy between previous works and the present study might be the

different tin concentrations within the ITO nanowires. Our highly conductive ITO nanowires also exhibit metallic behaviors, as shown in the temperature dependence data of Figure 5d. Since the lowest value of ITO resistivity at RT is 7.7 $\times 10^{-5}$ Ω cm in an epitaxial ITO single-crystal film grown on a YSZ substrate,[41] our averaged resistivity value of 2.1 $\times 10^{-4}$ Ω cm with almost 20% of 10^{-5} Ω cm range conductivity seems to be already quite low but can be further enhanced by optimizing and enhancing tin incorporation into ITO nanowires. To improve further the electrical conductivity of ITO nanowires, it would be a key issue to enhance not only the carrier concentration via increasing tin concentrations but also the mobility by an appropriate passivation of the nanowire surface.

CONCLUSION

In summary, we demonstrate a crucial role of preferential indium nucleation on the electrical conductivity of VLS grown ITO nanowires using gold catalysts. In spite of the fact that the vapor pressure of tin is lower than that of indium, we found that the indium concentration within the nanowires is always higher than the nominal composition. Thus, a VLS growth of ITO through gold catalysts significantly differs from ITO film formations due to the difference between the two metal elements on the nucleation probability at the LS interface. Furthermore, we demonstrate that the conductivity of ITO nanowires can be increased by considering the tin incorporation dynamics during ITO nanowire formation. We believe that the present findings will be a foundation to design and tailor novel multicomponent VLS nanowires.

ASSOCIATED CONTENT

Supporting Information

Temperature dependence data of vapor pressures for In, Sn, Sb, and Ta. This material is available free of charge via the Internet at http://pubs.acs.org.

AUTHOR INFORMATION

Corresponding Author

yanagi32@sanken.osaka-u.ac.jp; kawai@sanken.osaka-u.ac.jp

Notes

The authors declare no competing financial interest.

ACKNOWLEDGMENTS

This study was supported by NEXT. T.K. was supported by the FIRST program. A part of this work was supported by the "Low-Carbon Research Network (Handai satellite)" of the Ministry of Education, Culture, Sports, Science and Technology (MEXT), Japan.

REFERENCES

(1) Wagner, R. S.; Ellis, W. C. *Appl. Phys. Lett.* **1964**, *4*, 89.
(2) Morales, A. M.; Lieber, C. M. *Science* **1998**, *279*, 208.
(3) Huang, M. H.; Mao, S.; Feick, H.; Yan, H.; Wu, Y.; Kind, H.; Weber, E.; Russo, R.; Yang, P. *Science* **2001**, *292*, 1897.
(4) Dai, Z. R.; Pan, Z. W.; Wang, Z. L. *Adv. Funct. Mater.* **2003**, *13*, 9.
(5) Kolmakov, A.; Moskovits, M. *Annu. Rev. Mater. Res.* **2004**, *34*, 151.
(6) Shen, G.; Chen, P. C.; Ryu, K.; Zhou, C. *J. Mater. Chem.* **2009**, *19*, 828.
(7) Yu, H. K.; Dong, W. J.; Jung, G. H.; Lee, J. L. *ACS Nano* **2011**, *5*, 8026.
(8) O'Dwyer, C.; Szachowicz, M.; Visimberga, G.; Lavayen, V.; Newcomb, S. B.; Torres, C. M. S. *Nat. Nanotechnol.* **2009**, *4*, 239.
(9) Hu, L. B.; Kim, H. S.; Lee, J. Y.; Peumans, P.; Cui, Y. *ACS Nano* **2010**, *4*, 2955.
(10) Algra, R. E.; Verheijen, M. A.; Feiner, L. F.; Immink, G. G. W.; van Enckevort, W. J. P.; Vlieg, E.; Bakkers, E. P. A. M. *Nano Lett.* **2011**, *11*, 1259.
(11) Dubrovskii, V. G.; Sibirev, N. V.; Harmand, J. C.; Glas, F. *Phys. Rev. B* **2008**, *78*, 235301.
(12) Wen, C. Y.; Tersoff, J.; Reuter, M. C.; Stach, E. A.; Ross, F. M. *Phys. Rev. Lett.* **2010**, *105*, 195502.
(13) Oh, S. H.; Chisholm, M. F.; Kauffmann, Y.; Kaplan, W. D.; Luo, W. D.; Ruhle, M.; Scheu, C. *Science* **2010**, *330*, 489.
(14) Klamchuen, A.; Yanagida, T.; Nagashima, K.; Seki, S.; Oka, K.; Taniguchi, M.; Kawai, T. *Appl. Phys. Lett.* **2009**, *95*, 053105.
(15) Klamchuen, A.; Yanagida, T.; Kanai, M.; Nagashima, K.; Oka, K.; Seki, S.; Suzuki, M.; Hidaka, Y.; Kai, S.; Kawai, T. *Appl. Phys. Lett.* **2011**, *98*, 053107.
(16) Lide, D. R. *CRC Handbook of Chemistry and Physics: A Ready-Reference Book of Chemical and Physical Data*, 84th ed.; Lide, D. R., Ed.; CRC Press: Boca Raton, FL, 2003.
(17) Nagashima, K.; Yanagida, T.; Oka, K.; Tanaka, H.; Kawai, T. *Appl. Phys. Lett.* **2008**, *93*, 153103.
(18) Nagashima, K.; Yanagida, T.; Tanaka, H.; Kawai, T. *Appl. Phys. Lett.* **2007**, *90*, 233103.
(19) Zhuge, F.; Yanagida, T.; Nagashima, K.; Yoshida, H.; Kanai, M.; Xu, B.; Klamchuen, A.; Meng, G.; He, Y.; Rahong, S.; Li, X. M.; Suzuki, M.; Kai, S.; Takeda, S.; Kawai, T. *J. Phys. Chem. C* **2012**, *116*, 24367.
(20) Nagashima, K.; Yanagida, T.; Tanaka, H.; Seki, S.; Saeki, A.; Tagawa, S.; Kawai, T. *J. Am. Chem. Soc.* **2008**, *130*, 5378.
(21) Meng, G.; Yanagida, T.; Nagashima, K.; Yanagishita, T.; Kanai, M.; Oka, K.; Klamchuen, A.; Rahong, S.; Horprathum, M.; Xu, B.; Zhuge, F.; He, Y.; Masuda, H.; Kawai, T. *RSC Adv.* **2012**, *2*, 10618.
(22) Oka, K.; Yanagida, T.; Nagashima, K.; Kawai, T.; Kim, J. S.; Park, B. H. *J. Am. Chem. Soc.* **2010**, *132*, 6634.
(23) Oka, K.; Yanagida, T.; Nagashima, K.; Tanaka, H.; Kawai, T. *J. Am. Chem. Soc.* **2009**, *131*, 3434.
(24) Nagashima, K.; Yanagida, T.; Oka, K.; Taniguchi, M.; Kawai, T.; Kim, J. S.; Park, B. H. *Nano Lett.* **2010**, *10*, 1359−1363.
(25) Nagashima, K.; Yanagida, T.; Oka, K.; Kanai, M.; Klamchuen, A.; Kim, J. S.; Park, B. H.; Kawai, T. *Nano Lett.* **2011**, *11*, 2114−2118.
(26) Kuykendall, T.; Ulrich, P.; Aloni, S.; Yang, P. *Nat. Mater.* **2007**, *6*, 951.
(27) Higgins, J. M.; Carmichael, P.; Schmitt, A. L.; Lee, S.; Degrave, J. P.; Jin, S. *ACS Nano* **2011**, *5*, 3268.
(28) Singh, A. K.; Janotti, A.; Scheffler, M.; Van de Walle, C. G. *Phys. Rev. Lett.* **2008**, *101*, 055502.
(29) Pan, S. S.; Li, G. H. *Recent Pat. Nanotechnol.* **2011**, *5*, 138.
(30) Heward, W. J.; Swenson, D. J. *J. Mater. Sci.* **2007**, *42*, 7135.
(31) Shannon, R. D. *Acta Crystallogr., Sect. A* **1976**, *32*, 751.
(32) Liu, B. D.; Bando, Y.; Liu, L. Z.; Zhao, J. J.; Masanori, M.; Jiang, X.; Golberg, D. *Nano Lett.* **2013**, *13*, 85.
(33) Gao, J.; Lebedev, O. I.; Turner, S.; Li, Y. F.; Lu, Y. H.; Feng, Y. P.; Boullay, P.; Prellier, W.; van Tendeloo, G.; Wu, T. *Nano Lett.* **2012**, *12*, 275.
(34) Karazhanov, S. Z.; Ravindran, P.; Grossner, U. *Thin Solid Films* **2011**, *519*, 6561.
(35) Klamchuen, A.; Yanagida, T.; Kanai, M.; Nagashima, K.; Oka, K.; Kawai, T.; Suzuki, M.; Hidaka, Y.; Kai, S. *Appl. Phys. Lett.* **2010**, *97*, 073114.
(36) Suzuki, M.; Hidaka, Y.; Yanagida, T.; Klamchuen, A.; Kanai, M.; Kawai, T.; Kai, S. *Phys. Rev. E* **2011**, *83*, 061606.
(37) Wan, Q.; Song, Z. T.; Feng, S. L.; Wang, T. H. *Appl. Phys. Lett.* **2004**, *85*, 4759.
(38) Wan, Q.; Dattoli, E. N.; Fung, W. Y.; Guo, W.; Chen, Y. B.; Pan, X. Q.; Lu, W. *Nano Lett.* **2006**, *6*, 2909.
(39) Gao, J.; Chen, R.; Li, D. H.; Jiang, L.; Ye, J. C.; Ma, X. C.; Chen, X. D.; Xiong, Q. H.; Sun, H. D.; Wu, T. *Nanotechnology* **2011**, *22*, 195706.

(40) Park, K. S.; Choi, Y. J.; Kang, J. G.; Sung, Y. M.; Park, J. G. *Nanotechnology* **2011**, *22*, 285712.
(41) Ohta, H.; Orita, M.; Hirano, M.; Tanji, H.; Kawazoe, H.; Hosono, H. *Appl. Phys. Lett.* **2000**, *76*, 2740.